Quaternary Structure of the Severe Acute Respiratory Syndrome (SARS) Coronavirus Main Protease†

Chi-Yuan Chou,‡ Hui-Chuan Chang,§ Wen-Chi Hsu,§ Tien-Zheng Lin,§ Chao-Hsiung Lin,§ and Gu-Gang Chang*,§

Graduate Institute of Life Sciences, National Defense Medical Center, and Faculty of Life Sciences, Institute of Biochemistry, Structural Biology Program, and Proteome Research Center, National Yang-Ming University, Taipei, Taiwan

Received May 14, 2004; Revised Manuscript Received September 11, 2004

ABSTRACT: SARS (severe acute respiratory syndrome) has been one of the most severe viral infectious diseases last year and still remains as a highly risky public health problem around the world. Exploring the types of interactions responsible for structural stabilities of its component protein molecules constitutes one of the approaches to find a destabilization method for the virion particle. In this study, we performed a series of experiments to characterize the quaternary structure of the dimeric coronavirus main protease (M^{pro}, $3CL^{pro}$). By using the analytical ultracentrifuge, we demonstrated that the dimeric SARS coronavirus main protease exists as the major form in solution at protein concentration as low as 0.10 mg/mL at neutral pH. The enzyme started to dissociate at acidic and alkali pH values. Ionic strength has profound effect on the dimer stability indicating that the major force involved in the subunit association is ionic interactions. The effect of ionic strength on the protease molecule was reflected by the drastic change of electrostatic potential contour of the enzyme in the presence of NaCl. Analysis of the crystal structures indicated that the interfacial ionic interaction was attributed to the Arg-4···Glu-290 ion pair between the subunits. Detailed examination of the dimer−monomer equilibrium at different pH values reveals apparent pK_a values of 8.0 ± 0.2 and 5.0 ± 0.1 for the Arg-4 and Glu-290, respectively. Mutation at these two positions reduces the association affinity between subunits, and the Glu-290 mutants had diminished enzyme activity. This information is useful in searching for substances that can intervene in the subunit association, which is attractive as a target to neutralize the virulence of SARS coronavirus.

In early 2003, the outbreak of severe acute respiratory syndrome (SARS)[1] had raised a worldwide public health crisis (*1*−*3*). A new type of coronavirus (CoV) was soon identified as the etiological agent for SARS (*4*, *5*). The genome organization is very similar to that of other coronaviruses, but phylogenetic analysis of the viral protein and sequence comparisons indicate that SARS-CoV does not resemble any of the previously characterized coronaviruses (*4*−*8*). At present, there is no effective therapy for this disease. Structural information about the viral proteins could help to understand their functional role and thus provides a basis for designing an inhibitor against the virus (*9*−*11*).

Many viruses encode one or more proteases. These proteases are involved in the viral life cycle, maturation of precaspsid, and production of new infectious virions. The viral protease inhibitors thus have an important clinical relevance in the treatment of various viral infectious diseases (*12*−*17*). Among the viral proteases, the 33.8 kDa 3′-proximal region chymotrypsin-like protease ($3CL^{pro}$) plays a major role in the proteolytic processing of the virion polyproteins; it is also called the virion main protease (M^{pro}).

The crystal structure of SARS-CoV main protease represents the first solved structure for any SARS-CoV proteins (Figure 1A) (*18*). The protein is a homodimer with two subunits arranged perpendicular to each other (Figure 1B). Each monomer of the enzyme constitutes three structural domains. The active site is located at the interface between domains I and II, which have similar folding scaffold with other viral chymotrypsin-like proteases (*19*−*21*). Specifically for the coronavirus main proteases, the SARS-CoV main protease contains a third globular helical domain linked to the domain II by a long loop (*18*−*21*). The role of domain III in the CoV main protease seems to relate to the dimer formation (*22*). The N-terminus of the protease (N-finger) extends from domain I toward domain III and forms intensive interactions with subunit B. The side chain of Arg-4 at the N-finger fits into a pocket of subunit B and forms a salt bridge with Glu-290, which constitutes one of the major

† This work was supported by the National Science Council, ROC (SARS Project, Grant NSC 92-2751-B-010-004-Y).

* To whom correspondence should be addressed. Tel: 886-2-2820-1854. Fax: 886-2-2820-1886. E-mail: ggchang@ym.edu.tw.

‡ National Defense Medical Center.

§ National Yang-Ming University.

[1] Abbreviations: SARS, severe acute respiratory syndrome; CoV, coronavirus; WT, wild-type; R4A, single mutant of SARS-CoV main protease with arginine at position 4 replaced by alanine; E290A, single mutant of SARS-CoV main protease with glutamate at position 290 replaced by alanine; R4A/E290A, double mutant of SARS-CoV main protease with both arginine-4 and glutamate-290 replaced by alanine; 3CLc, truncation mutant of SARS-CoV main protease with the whole C-terminal domain III deleted; PCR, polymerase chain reaction; CD, circular dichroism; AUC, analytical ultracentrifuge; SDS/PAGE, sodium dodecyl sulfate/polyacrylamide gel electrophoresis; IPTG, isopropyl-1-thio-β-D-galactoside; PBS, phosphate-buffered saline.

10.1021/bi0490237 CCC: $27.50
Published on Web 10/30/2004

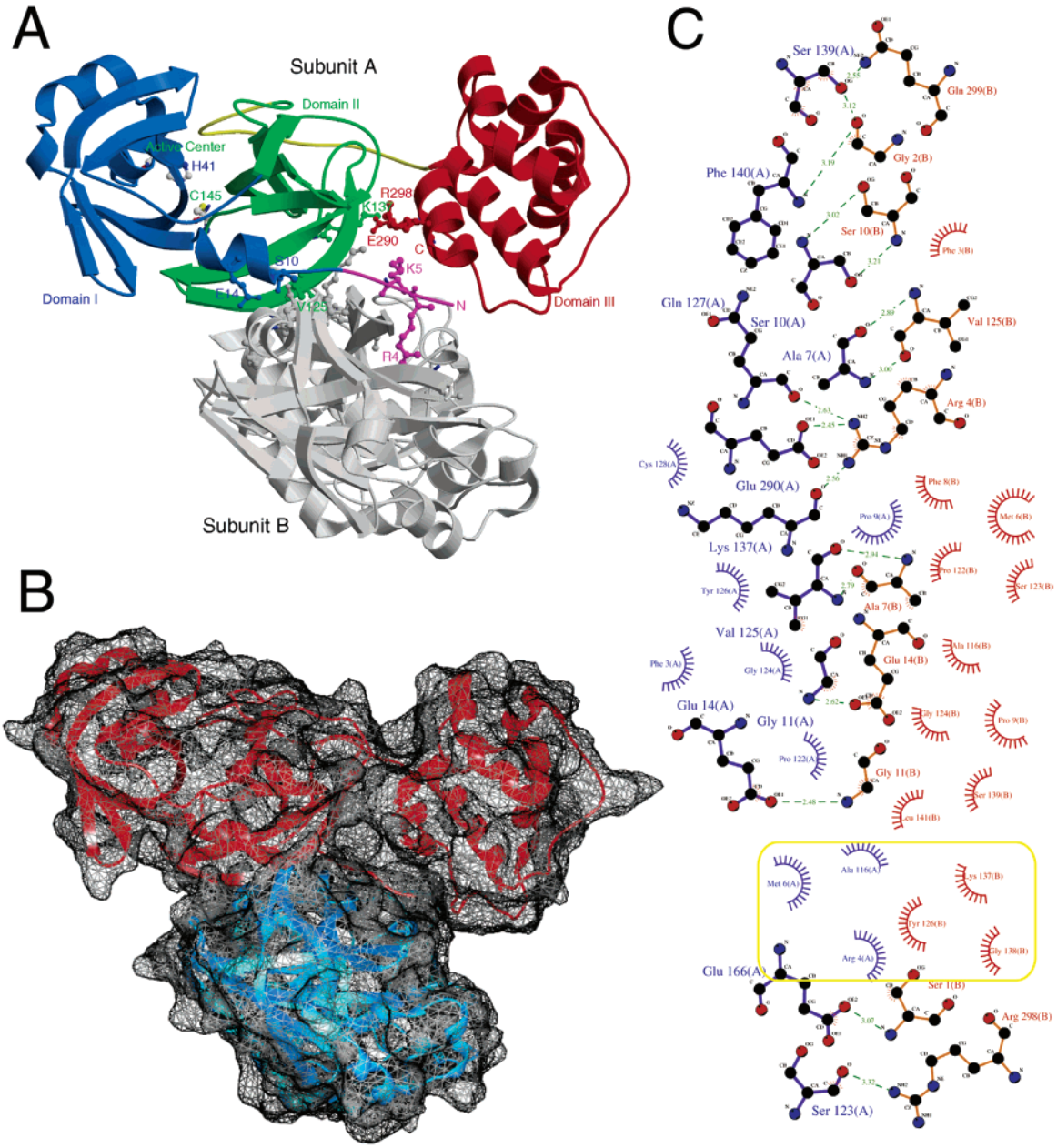

FIGURE 1: Crystal structure of the SARS-CoV main protease. Panel A shows a ribbon diagram for the crystal structure of the protease (pdb code 1UJ1). In one of the subunits of the dimeric enzyme, the three structural domains are shown in blue for domain I (residues 8−99), green for domain II (residues 100−183), and red for domain III (residues 200−306). The N-terminal finger (residues 1−7, in pink) stretches into the subunit interfacial region is heavily involved in the interactions of subunits. There is also a long loop (residues 184−199, in yellow) that links domains II and III. The second subunit is shown in gray. The catalytic dyad, His-41 and Cys-145 (in CPK), and some of the contacting residues in the subunit interface are shown in the bond model. This figure was generated with Molscript (*53*) and Raster3D (*54*). Panel B shows a surface model of the enzyme. The two subunits (in red and blue) are in the same orientation as in shown in panel A in which domain I of subunit B is located in front, while domain III is behind the page. Panel C shows a Dimplot (*55*) of the interfacial binding modes at pH 7.6. The blue bonds and residues belong to subunit A and those in red to Subunit B. The dashed lines represent the hydrogen bonds and spoked arcs represent the hydrophobic interactions. The hydrophobic interactions in the yellow circle are not observed in the crystal structures at pH 6.0 or 8.0.

interactions between the two subunits as explored in this article.

Besides the Arg-4···Glu-290 ion pair, the subunit interfacial region of the SARS-CoV main protease contains hydrophobic interactions and hydrogen bonds (Figure 1C). Dissociation of the dimeric protease seems to result in an enzymatically active monomer (*22*, *23*), and the dimeric form has been proposed to be the biological function form (*20*). The subunit interfacial region of the main protease has been suggested to be a possible target for rational drug design against the SARS-CoV (*22*, *23*). For this reason, it is essential to understand the quaternary structure of the enzyme in solution. The present article aims to address this important issue.

EXPERIMENTAL PROCEDURES

Plasmids. The pET-29a (+) (Novagen) vectors were used, which carry a C-terminal His_6·tag sequence and multiple cloning sites below the f1 origin. This kanamycin-resistant vector was transformed into the BL21 (DE3) strain of

Escherichia coli. The expression of enzyme was induced with 1.0 mM isopropyl-1-thio-β-D-galactoside (IPTG), and the cells were harvested after 3 h at 37 °C.

Construction of WT SARS-CoV Main Protease and 3CLc Expression Vectors. The plasmid containing the full-length protease was provided by the Genome Research Center, National Yang-Ming University, Taipei, Taiwan, Republic of China. The cDNAs of the main protease and the domain III-deletion mutant (3CLc) were amplified by polymerase chain reaction (PCR). The forward primer for both cDNAs is 5′-GGTGGTCATATGAGTGGTTTTAGG. The reverse primer for the main protease is 5′-AACTCGAGGGTAACACCAGAG, and that for 3CLc is 5′-AACTCGACTATGGTTGTGTCTG. Both PCR products were digested with *Bgl*II and *Xho*I and divided into 168-bp (near 5′-end) and 747- or 432-bp (near 3′-end) fragments. The 168-bp fragment was then digested with *Nde*I. Finally, the 168-bp *Nde*I−*Bgl*II and the 747-bp or 432-bp *Bgl*II−*Xho*I fragments were coligated to a 5.2 kb *Nde*I−*Xho*I pET-29a (+) fragment. These in turn resulted in a 6.2 kb pET-SARS-CoV main protease vector or a 5.8 kb pET-3CLc vector, in which both cDNAs were driven by the T7 promoter and C-terminal-fused with His_6tag sequence.

Construction of the R4A, E290A, and R4A/E290A Mutant Expression Vectors. Site-directed mutagenesis was used to construct the pET-R4A, pET-E290A, and pET-R4A/E290A vectors (*24*). The forward primer for R4A was 5′-ATGAGTGGTTTTGCGAAAATGGCATTCCC, and the reverse primer was 5′-GGGAATGCCATTTTCGCAAAACCACTCAT. The forward primer for E290A was 5′-ATTTTAGAAGATGCGTTTACACCATTTG, and the reverse primer was 5′-CAAATGGTGTAAACGCATCTTCTAAAT. Briefly, pET-SARS-CoV main protease vectors were used as templates, and the desired primers were used to mutate the Arg-4 codon to an Ala-4 codon or the Glu-290 codon to an Ala-290 in the process of PCR using DNA polymerase *Pfu* (Promega). After 16−18 rounds of temperature cycling, the mutated plasmids containing staggered nicks were generated. The PCR products were then treated with *Dpn*I (New England Biolabs) to digest the pET-SARS-CoV main protease templates. Finally, the nicked vector DNA incorporating the desired mutations was transformed into *E. coli*, and their DNA sequence was checked by autosequencing. The pET-R4A vectors were used as the template to construct pET-R4A/E290A vectors. The entire cDNA was also sequenced to exclude any unexpected mutations resulting from in vitro DNA polymerase extension. The absence of adventitious base changes was verified in all recombinant proteases. All manipulations were performed in a P2 laboratory.

Purification of SARS-CoV Main Protease. After being induced by IPTG at 37 °C for 3 h, the cells were centrifuged at 6000 × *g* (4 °C) for 10 min. The supernatant was removed, and the cell pellets were suspended in the binding buffer (containing 4 mM imidazole, 300 mM NaCl, and 20 mM Tris-Cl, pH 7.9). The cells were then sonicated by 60 10-s bursts at 300 W with a 10 s cooling period between each burst. The lysate was centrifuged at 10 000 × *g* (4 °C) for 25 min to pellet the cellular debris. One milliliter of the binding buffer-equilibrated Ni−NTA agarose slurry (Qiagen) was then added to the clear lysate, and the solution was mixed gently at 4 °C for 60 min to equilibrium. The lysate−Ni−NTA mixture was then loaded into a column and washed with the washing buffer (containing 30 mM imidazole, 300 mM NaCl, and 20 mM Tris-Cl, pH 7.9). Finally, the main protease was eluted with an elution buffer (containing 400 mM imidazole, 300 mM NaCl, and 20 mM Tris-Cl, pH 7.9).

Samples from the purification steps were subjected to electrophoresis with a gradient of 4−12% polyacrylamide gel in the presence of sodium dodecyl sulfate (SDS/PAGE) in a Bio-Rad protein II system to check the homogeneity.

Buffer Change of the SARS-CoV Main Protease. The purified enzyme was concentrated by Amicon Ultra-4 centrifugal filter devices (Millipore) with molecular cutoff at 10 kDa. The purified enzyme was concentrated to 5−10 mg/mL and then diluted to 0.5−1.0 mg/mL in PBS (containing 4 mM NaH_2PO_4, 16 mM Na_2HPO_4, and 150 mM NaCl, pH 7.3), which replaced the elution buffer after five times concentration−dilution procedure.

For pH studies, PBS solutions with different pH values were prepared by mixing equal molar solutions of Na_2HPO_4 and NaH_2PO_4 to the desired pH value. The pH was adjusted with equal molar H_3PO_4, if necessary. In this way, the same ionic strength was maintained in all buffer solutions with various pH values. Aliquots of the enzyme solution were added into the buffer solutions, and the final pH values were recorded.

The pH−pK_a profile was fitted to the following equation for two protonation sites (eq 1):

$$\log K_a = \log \frac{K_A}{1 + \frac{[H^+]}{K_{a_1}} + \frac{K_{a_2}}{[H^+]}} \quad (1)$$

in which K_a is the observed dissociation constant at various pH values. K_A is the pH-independent limiting K_a value. K_{a_1} and K_{a_2} are the dissociation constants for the amino acid residues responsible for the two ionization steps.

Circular Dichroism and Fluorescence Analyses. CD measurements were performed in a Jasco J-810 spectropolarimeter at 25 °C under constant N_2 flush, using a 1 mm path-length cell. The secondary structural contents were estimated by the online DICHROWEB server (web site, http://public-1.cryst.bbk.ac.uk/cdweb/html/, accessed on August 10, 2004) (*25*, *26*) using the implemented CDSSTR program.

Fluorescence emission spectra of the recombinant SARS-CoV main proteases with excitation wavelength at 280 nm were obtained in a Perkin-Elmer LS 50B luminescence spectrometer at 25 °C. All spectra were corrected for the buffer absorption.

Analytical Ultracentrifugation Analysis. The molar mass and sedimentation coefficient of the protease were analyzed by a Beckman-Coulter XL-A analytical ultracentrifuge. Prior to the experiments, samples in the buffer were diluted to various protein concentrations. Samples (400 μL) and reference (440 μL) solutions were loaded to double-sector centerpieces and mounted in a Beckman An-50 Ti rotor. Experiments were performed at 20 °C with a rotor speed of 42 000 rpm. Absorbance of the sample at 230 or 280 nm was monitored in a continuous mode with a time interval of 480 s and a step size of 0.002 cm without averaging. Multiple scans at different time points were fitted to a continuous size

distribution by using the SEDFIT program (*27*−*30*). Dissociation constant of the dimer−monomer equilibrium was calculated by global fitting of the sedimentation data with the SEDPHAT program (*31*). A partial specific volume of 0.7294 and extinction coefficient of 32 495 M^{-1} cm^{-1} at 280 nm (0.942 mg/mL) were used in all calculations. The solvent density and viscosity were corrected with the SEDNTERP program (website, http://www.jphilo.mailway.com/default.htm, accessed on August 10, 2004). All samples were visually checked for clarity after ultracentrifugation to ensure that there was no indication of precipitation due to unfolding of the protein.

Analytical Size-Exclusive Chromatography. Size-exclusive chromatographic experiments were performed using an Amersham Biotech ÄKTA purifier system with a Superose 12 (10/300) column preequilibrated with PBS of the corresponding pH values. Purified enzyme (0.1 or 0.2 mL in PBS) was injected into the column. The elution was carried out at a flow rate of 0.8 mL/min, and the absorbance at 280 or 230 nm was monitored continuously. Proteins with known M_r were analyzed under the identical conditions to evaluate the molecular mass at each pH value.

Protease Activity Assay. The proteolytic activity of the SARS-CoV main protease was measured by a continuous fluorescence-based peptide cleavage assay method similar to those used for human cytomegalovirus protease (*32*, *33*). The substrate used was an internally quenched fluorogenic 11-mer peptide, *ortho*-aminobenzoic acid-Thr-Ser-Ala-Val-Leu-Gln-Ser-Gly-Phe-Arg-Lys-2,4-dinitrophenyl amide (Genemed Synthesis Inc., South San Francisco, CA), which mimics the N-terminal autocleavage site of the SARS-CoV main protease and cuts at the Gln↓Ser site (*22*, *23*). The peptide substrate was dissolved in dimethyl sulfoxide to prepare a 5 mM stock solution and then diluted with buffer A (containing 10 mM phosphate buffer, 150 mM NaCl, and 2 mM 2-mercaptoethanol, pH 7.6) to the desired concentrations.

The reaction mixture used for the enzyme activity assay contained 0.5−25 μM substrate in buffer A in a total volume of 1 mL. After addition of the enzyme into the reaction mixture, the increase of fluorescence at 423 nm (excited at 321 nm) was continuously monitored at 30 °C with a Perkin-Elmer LB 50 luminescence spectrometer. The slope of the line was taken as the initial enzyme activity, which was linearly correlated to the enzyme amount added in the reaction mixture in the range used in our experiments. One unit of enzyme activity was defined as the fluorescence units per minute.

Steady-state kinetic parameters of the enzyme were determined by fitting the initial velocity data to a Michaelis−Menten equation (eq 2)

$$v = \frac{V_{max}[S]}{K_m + [S]} \quad (2)$$

in which v is the initial reaction rate, V_{max} is the maximum reaction rate, [S] denotes the substrate concentration, and K_m is the Michaelis constant for the peptide substrate.

Peptide Cleavage. Proteolysis activity of the SARS-CoV main protease was confirmed by peptide cleavage assay and analyzed by reverse-phase high-performance liquid chromatography (HPLC). The peptide substrate of 10 μM was incubated with the enzyme (8 μM) in PBS (pH 7.6) at room temperature for 2 h. The cleavage reaction was stopped by the addition of 0.1% trifluoroacetic acid solution, and the hydrolytic products were then analyzed with a Cosmosil 5C18-AR-II column (4.6 mm × 250 mm, Nacalai tesque Co.) using an Amersham Biotech ÄKTA purifier system. Cleavage products were resolved using a 25-min 0−50% linear gradient of acetonitrile in 0.1% trifluoroacetic acid.

Calculation of Electrostatic Potential. The electrostatic potentials of the protease were calculated using the SPOCK program (web site, http://mackerel.tamu.edu/spock, accessed on August 12, 2004). The nonlinear Poisson−Boltzmann equation was solved for SARS-CoV main protease at three pH values, 1UJ1 for pH 6.0, 1UK3 for pH 7.6, and 1UK2 for pH 8.0 (*18*). The charges and dielectric boundary were mapped into a cubic grid (65 grid points × 65 grid points × 65 grid points). An internal relative permittivity constant of 2 was accepted. Dielectric permittivity for the solvent was 80. The salt concentration was taken at 0, 0.15, and 4 M, and the temperature was set at 298.16 K.

RESULTS

Purification of the Recombinant SARS-CoV Main Protease. The recombinant SARS-CoV main proteases (WT and mutants) were successively cloned, expressed, and purified as a soluble form. The whole expression and purification procedure was completed in 2 days with a yield of purified enzyme of 6−8 mg per liter of the cell culture medium. A single affinity column has achieved the purification work, which greatly facilitated the structure−function studies. A second gel filtration chromatography step seemed not necessary as other protocols suggested (*23*, *34*). SDS/PAGE analysis indicated that all recombinant enzymes are nearly homogeneous in solution (Figure 2). All proteins except the overexpressed SARS-CoV main protease flow through the column unbound. In WT and Arg-4 or Glu-290 mutants or both, a highly purified protein band with a M_r of approximately 30 kDa was obtained, in agreement with the molar mass of SARS-CoV main protease calculated from the amino acid sequence (33.8 kDa). The domain III-truncated mutant 3CLc showed a M_r of 22 kDa, which is also expected from the theoretical value (M_r 21.7 kDa) (Figure 2).

Characterization of the Recombinant SARS-CoV Main Protease. The recombinant SARS-CoV main proteases (WT and mutants) were examined by CD and fluorescence analyses. The overall CD spectra of all recombinant SARS-CoV main proteases seemed to be similar (Figure 3A) except in the 190−200 nm range, which is an unreliable region because of high noise level. These results indicate that the overall structure of the enzyme did not alter after mutation. However, small structural changes do exist as reflected in the secondary structural estimation by the DICHROWEB server (*25*, *26*). The normalized root-mean-square deviation (NRMSD) values of the data fitting for WT, R4A, E290A, and R4A/E290A were 0.025, 0.018, 0.023, and 0.078, respectively, which were all <0.1 and thus showed excellent goodness of the fit parameters (*35*). The helical contents of the WT, R4A, E290A, and R4A/E290A were 0.34, 0.35, 0.37, and 0.24, respectively; and the β-sheet contents were 0.13, 0.18, 0.24, and 0.23, respectively. The β-turn contents

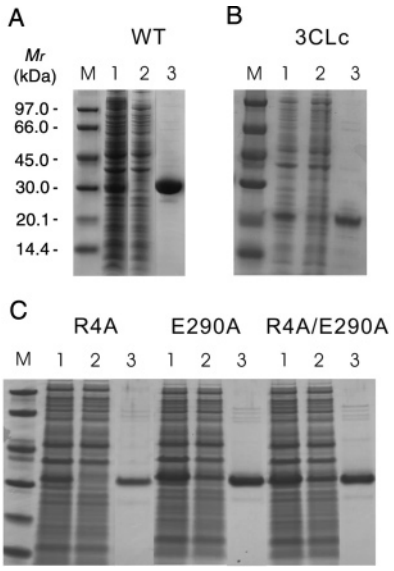

FIGURE 2: Expression and purification of SARS-CoV main protease in the *Escherichia coli* cells: SDS−PAGE (4−12% gradient gel) of the recombinant SARS-CoV main protease for (A) full-length wild-type, (B) 3CLc domain III-truncated mutant, and (C) single and double mutants of the Arg-4···Glu-290 ion pair. Lane M contains the following M_r markers: phosphorylase b, 97 kDa; bovine serum albumin, 66 kDa; ovalbumin, 45 kDa; carbonic anhydrase, 30 kDa; trypsin inhibitor, 20.1 kDa; α-lactalbumin, 14.4 kDa. Lane 1 is the crude cell extract. Lanes 2 and 3 are those of the flow-through and eluting fractions of the enzyme from the Ni−NTA affinity column.

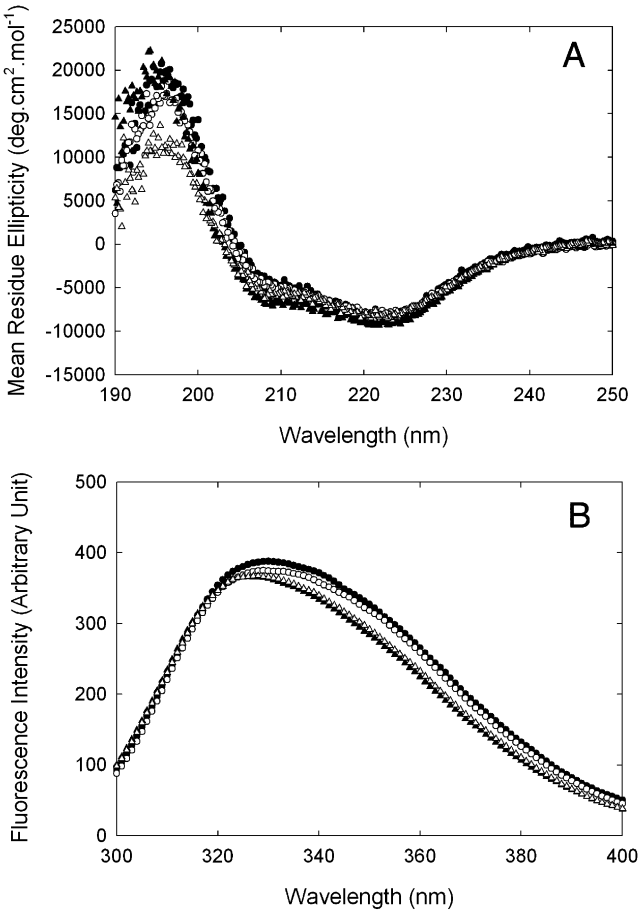

FIGURE 3: Biophysical characterization of the recombinant SARS-CoV main protease. CD spectra (A) and fluorescence emission spectra (B) were obtained for all recombinant SARS-CoV main proteases: (●) WT; (○) R4A; (▲) E290A; (△) R4A/E290A double mutant.

were 0.19, 0.19, 0.12, and 0.19, respectively, and the unordered structures were 0.27, 0.27, 0.26, and 0.34, respectively, for the WT, R4A, E290A, and R4A/E290A.

The fluorescence emission spectra of the recombinant SARS-CoV main proteases are shown in Figure 3B. The average emission wavelengths calculated by the method of Sanchez del Pino and Fersht (*36*) for the WT, R4A, E290A, and R4A/E290A were 342.3, 342.2, 340.4, and 340.7 nm, respectively.

Analytical Ultracentrifugation Analysis. The quaternary structural changes of the recombinant SARS-CoV main protease were examined by analytical ultracentrifugation (Figure 4). Most of the protease molecules sediments at 4.2 S (Figure 4D) corresponding to a species with molar mass of 68 kDa (Figure 4E), which was in excellent agreement with the molecular weight calculated from amino acid sequence of the dimer (67.6 kDa). There was a small peak at 2.4 S, corresponding to 34 kDa (monomer). At high protein concentrations, the monomer peak was diminished (Figure 4F,G). No aggregation was observed at sedimentation coefficient up to 20 S in all protein concentrations tested. The excellent matching of the experimental data points and the curve fitting results (Figure 4A), the randomly distributed residual values (Figure 4B), and the homogeneous bitmap picture (Figure 4C) all indicated that a highly reliable model for the sedimentation velocity experiments was obtained and the analytical ultracentrifugation was an excellent biophysical probe for accessing the quaternary structure of the enzyme.

The sedimentation velocity experiment was performed at a wide protein concentration range (0.1−1.5 mg/mL) (data not shown). There is a close correlation between the monomer−dimer distribution and protein concentration. Higher protein concentration favors dimer formation. This result indicates that an equilibrium dimer−monomer system exists in the solution. To have appreciable amount of monomer to detect for evaluating the dissociation constant of the SARS-CoV main protease under various conditions, in the following experiments, a low protein concentration (0.1 mg/mL, 1.44 μM) was used. The absorbance of 230 nm was used to increase the detection sensitivity.

Dependence of the Dissociation of Dimeric SARS-CoV Main Protease on Ionic Strength. To examine the possible effect of ionic strength on the quaternary structure of the dimeric SARS-CoV main protease, we performed the sedimentation velocity experiments by adding different amounts of NaCl in the protein solution. Figure 5 shows that the ionic strength has pronounced effect on the quaternary structure of the SARS-CoV protease. The enzyme has been dissociated in the presence of 150 mM NaCl. Complete dissociation of the dimeric SARS-CoV main protease was observed in 3 M NaCl.

The results of molar mass analysis indicated that the protease behaves anomalously in the absence of NaCl. The molar mass is underestimated in this case (Figure 5B). This could arise from the primary charge effect. Another implication is that salt has affected the molecular shape of the protease molecule in solution. The c(s) method used in SedFit program results in a "single" and "average" f/f_o (friction ratio)

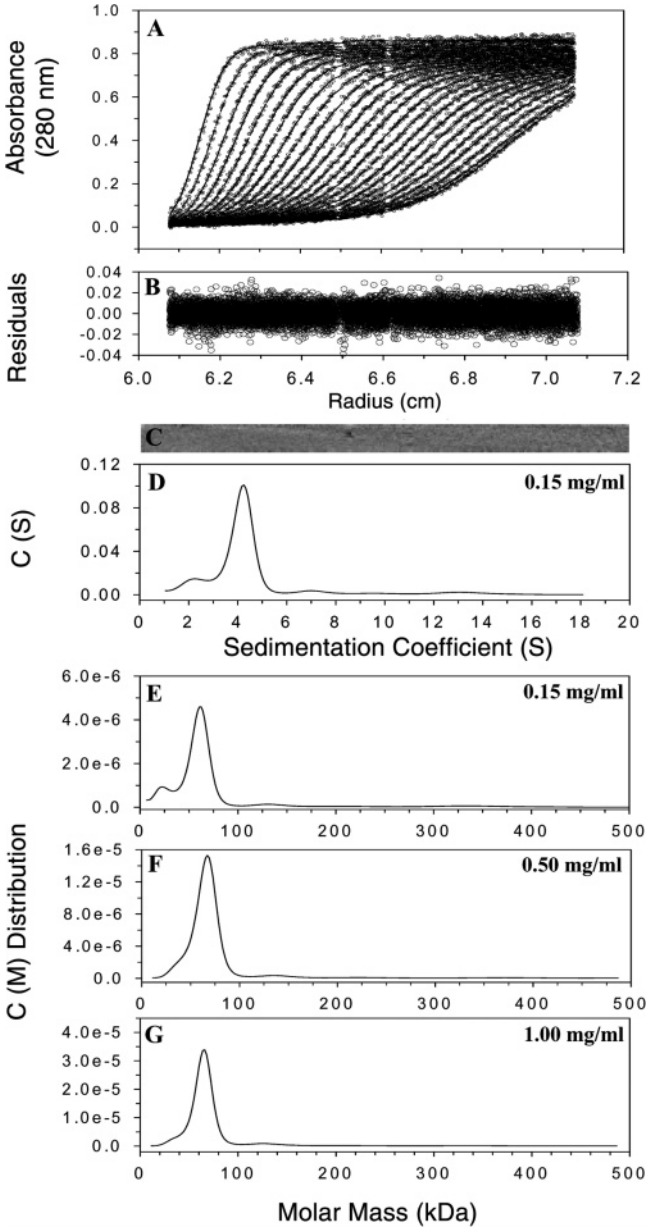

FIGURE 4: Sedimentation velocity experiments of the SARS-CoV main protease. The sedimentation of the enzyme under various conditions was analyzed with a Beckman-Coulter XL-A analytical ultracentrifuge with an An50Ti rotor. Panel A shows a typical trace of absorbance at 280 nm of the SARS-CoV main protease during the sedimentation velocity experiment. The symbols are experimental data, and the lines are computer-generated results by fitting the experimental data to the Lamm equation with SEDFIT program (*27*−*30*). Panel B shows the residuals of the model fitting of the data in panel A. Panel C shows the bitmap picture of the residual distribution. In panels A−C, the protein concentration was 1.0 mg/mL in 10 mM PBS (pH 7.3). Panel D shows the continuous sedimentation coefficient distribution of the enzyme at low protein concentration. Panels E−G show the continuous molar mass distribution of the enzyme at different protein concentrations.

parameter for all species in a sample. The f/f_o value is then used to transform the sedimentation coefficient distribution to a MW distribution. This approach is valid only if the shape does not change much. This assumption may not hold in our case.

In summary, the above data indicate the importance of ionic interaction in the subunit association. The effect of pH

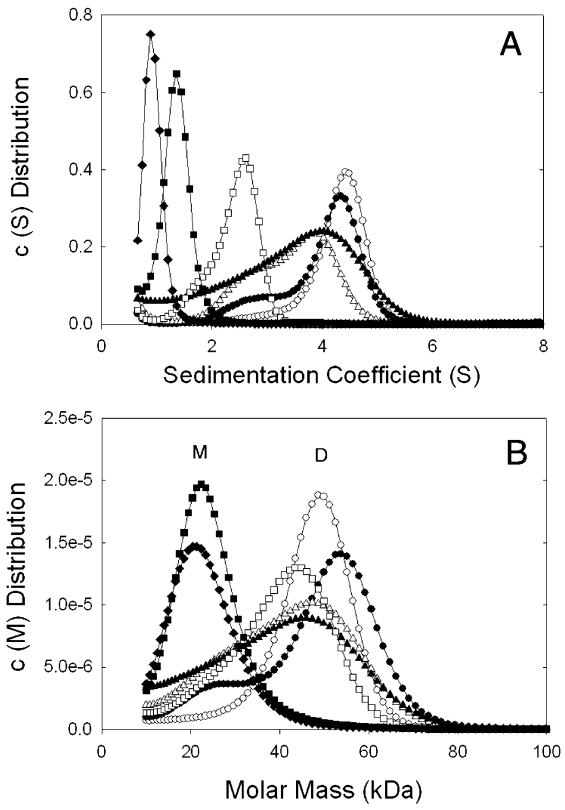

FIGURE 5: Effect of ionic strength on the quaternary structure of SARS-CoV main protease: (A) continuous sedimentation coefficient distribution, $c(s)$ and (B) continuous molar mass distribution, $c(M)$, of the SARS-CoV main protease (0.1 mg/mL, 1.44 μM) in 10 mM PBS (pH 8.0). The NaCl concentrations in the enzyme solutions are as follows: (○) 0; (●) 0.15; (△) 0.5; (▲) 1; (□) 2; (■) 3; (◆) 4 M.

on the quaternary structure stability was then examined in 10 mM PBS, which contained 150 mM NaCl.

Dependence of the Dissociation of Dimeric SARS-CoV Main Protease on pH. The crystal structures of the enzyme at pH 6.0, 7.6, and 8.0 were available (*18*). We have examined the quaternary structure of the enzyme at these pH values. Figure 6 shows that, under other identical conditions, the enzyme exists as a mixture of dimer and monomer at these pH values (Figure 6B−D). In an extreme acidic environment (pH 3.6), the enzyme was completely dissociated (Figure 6A). No aggregation was observed at pH 4.0−10.0.

To fully characterize the dimer−monomer equilibrium, we examined the dissociation of SARS-CoV main protease at different pH values between 3.6 and 10.0, and the dissociation constant of the dimer−monomer equilibrium was estimated by the SEDPHAT program (*31*). Figure 7A shows a typical global fitting of the data. The excellent fitting of the experimental data with the fitting curves and the randomly distributed residuals around zero indicate that the data are adequately described by the model (Figure 7A,B). Figure 7C shows the correlation between pH and the useful dissociation constants. From this plot, we reached the conclusion that two amino acid residues with apparent pK_a values of 5.0 ± 0.1 and 8.0 ± 0.2 are involved in the subunit association of the SARS-CoV main protease. The former must be deprotonated and the latter protonated for a stable association of the subunits.

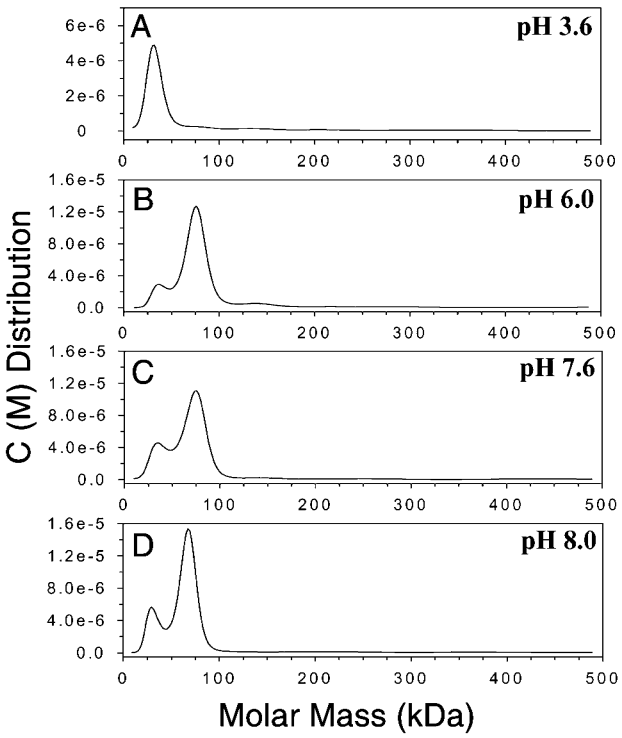

FIGURE 6: Effect of pH on the quaternary structure of the SARS-CoV main protease—continuous sedimentation coefficient distribution of the SARS-CoV main protease in 10 mM PBS. The pH values of the solution were as follows: (A) 3.6; (B) 6.0; (C) 7.6; (D) 8.0. The protein concentration was 0.1 mg/mL (1.44 μM) in 10 mM PBS. Absorbance at 230 nm was used to monitor the protein sedimentation.

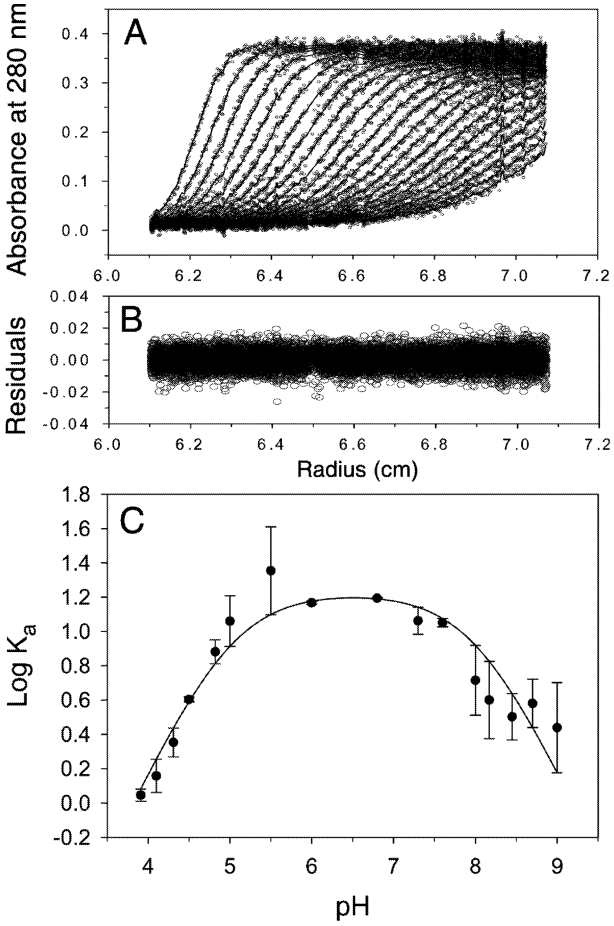

FIGURE 7: Dissociation of the SARS-CoV main protease in acidic and alkali environments. Panel A shows a typical trace of the absorbance at 230 nm of the SARS-CoV main protease at pH 5.5 in 10 mM PBS during the sedimentation velocity experiment. The symbols are experimental data, and the lines are computer-generated results by global fitting of the experimental data to a monomer−dimer self-association model by the SEDPHAT program (*31*). Panel B shows the residuals of the model fitting of the data in panel A. Panel C shows the correlation of the dimer−monomer equilibrium with pH. The protein concentration was 1.44 μM in 10 mM PBS. Open circles show the data obtained from the sedimentation velocity experiments. The line is the computer-generated results by fitting of the experimental data to a system with two ionizable groups. Error bars represent the fitting residuals.

Analytical Size-Exclusive Chromatography of the Dimeric SARS-CoV Main Protease. Since Fan et al. (*23*) had reported a monomeric species of the SARS-CoV main protease by size-exclusive chromatography at pH 6.0, we examined our recombinant SARS-CoV main protease under the same conditions on a Superose 12 column. The results shown in Figure 8 indicate that the enzyme existed as a main species of 45 kDa, which may be a mixture of dimer and monomer under various conditions. The monomer (about 20−25 kDa) alone was detected only in an extreme low pH environment.

Aggregation was observed at pH 3.6. This indicated that the dissociated monomer was partially unfolded in this extreme environment and thus prone to aggregate. The sedimentation data at the extreme pH values were discarded in the calculation of dissociation constant.

Effect of the Arg-4···Glu-290 Ion Pair Mutation on the Quaternary Structure of SARS-CoV Main Protease. The above results suggest the importance of ionic interaction in the dimer association of the SARS-CoV main protease. Structural studies of the enzyme point to the interfacial Arg-4···Glu-290 ion pair (*18*). To further characterize the role of this ion pair in the dimer stability of the enzyme, two single mutants (R4A and E290A) and a double mutant (R4A/E290A) were prepared and purified to near homogeneity (Figure 2C). Mutation at Arg-4 or Glu-290 increased the dissociation constant of the dimeric enzyme by 4.5- and 5.1-fold, respectively, compared to the WT enzyme. The R4A/E290A double mutant, however, reduced the difference to 3.4-fold only (Table 1). In a separate experiment performed at pH 7.6, as compared to WT, the dissociation constant increased by 5.1, 28.5, and 16.2-fold, respectively, for the R4A, E290A, and R4A/E290A mutants.

Effect of the Arg-4···Glu-290 Ion Pair Mutation on the Enzymatic Activity of SARS-CoV Main Protease. Peptide cleavage by the SARS main protease was demonstrated by HPLC (Figure 9A). The original substrate (peak 1) was identified by amino acid sequence analysis. The cleavage site was confirmed by MALDI-TOF mass spectrometry of the isolated products. The original uncleaved peptide substrate eluted at 29.8 mL. The N-terminal product (*ortho*-aminobenzoic acid-Thr-Ser-Ala-Val-Leu-Gln) eluted at 36.1 mL, and the C-terminal product (Ser-Gly-Phe-Arg-Lys-2,4-dinitrophenyl amide) eluted at 25.8 mL. The fluorogenic substrate provides a convenient assay method for the protease enzymatic activity. Figure 9B shows some of the fluorescence traces of the assay. The fluorescence enhancement was collinear with time for at least 15 min, which made the initial velocity (v) measurements accurate. There is a linear

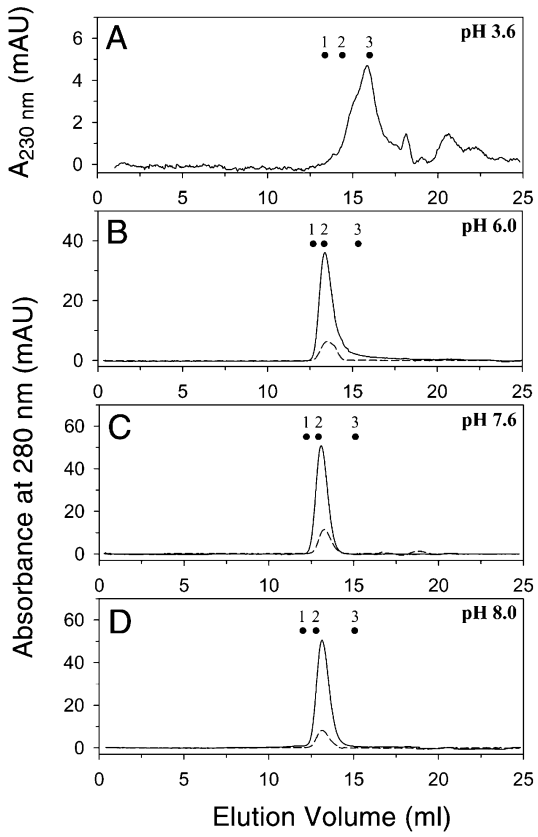

FIGURE 8: Size distribution of the SARS-CoV main protease analyzed by ÄKTA FPLC. The enzyme in various pH buffers was applied to the Superose 12 10/300 GL column preequilibrated with 10 mM PBS of the corresponding pH value. The enzyme was then eluted with the same buffer solution. The quaternary structure of the SARS-CoV main protease in various protein concentrations is shown in the varied retention volumes. Solid line corresponds to an injection of 0.1 mL of 1.0 mg/mL enzyme solution. Dashed line corresponds to injection of 0.2 mL of 0.1 mg/mL enzyme solution. Dots correspond to peak elution positions of 1 mg/mL (injection of 0.1 mL) molecular weight markers (Amersham Bioscience) as follows: (1) albumin, $M_r = 63.7$ kDa; (2) ovalbumin, $M_r = 48.6$ kDa; (3) ribonuclease A, $M_r = 15.7$ kDa.

Table 1: Kinetic and Equilibrium Parameters of the Recombinant SARS-CoV Main Protease

recombinant SARS-CoV main protease	kinetic parameters[a]			dissociation constant, K_d (nM)[b]
	K_m (μM)	V_{max} (U/nmol)	V_{max}/K_m (U/(nmol μM))	
wild-type	9.3 ± 1.5	8.0 ± 0.5	0.85 ± 0.10	190 ± 14
R4A	7.8 ± 3.6	6.0 ± 1.0	0.75 ± 0.25	870 ± 226
E290A				970 ± 437
R4A/E290A				640 ± 58

[a] Obtained from kinetic enzyme activity assay. Only those for the WT and R4A are reported. The other mutants have too little enzymatic activity to give reliable kinetic parameters. [b] The dimer−monomer equilibrium constants were obtained from sedimentation experiments at pH 8.0, calculated and corrected to the standard conditions of pure water at 20 °C by the SEDPHAT program (*31*). The results are presented as mean ± standard errors.

correlation between the initial velocity and enzyme amounts used in the reaction mixture (Figure 9C). The steady-state kinetics of the protease thus can be determined accurately. Similar approaches using other fluorogenic substrates were developed recently (*37*, *38*). The fluorescence method represents a much simpler assay procedure comparing to the

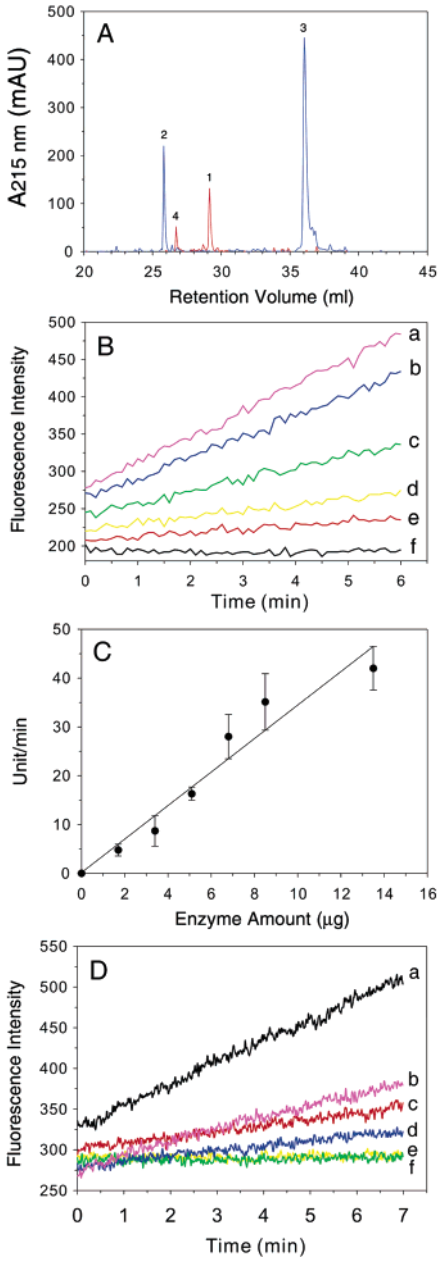

FIGURE 9: Cleavage of peptide substrate by the recombinant SARS-CoV main protease. The fluorogenic peptide *ortho*-aminobenzoic acid-Thr-Ser-Ala-Val-Leu-Gln-Ser-Gly-Phe-Arg-Lys-2,4-dinitrophenyl amide in 10 mM phosphate buffer (containing 150 mM NaCl and 2 mM 2-mercaptoethanol, pH 7.6) was incubated at 30 °C with WT or mutant SARS-CoV main protease. The fluorescence enhancement (excitation at 321 nm and emission at 423 nm) was monitored continuously to follow the peptide cleavage. The acidified reaction mixture was also analyzed by HPLC as described in Materials and Methods. Panel A shows HPLC profiles of the cleavage reaction by SARS main protease: red, 0 min; blue, 2 h incubation. Peak 1 was the original peptide. Peaks 2 and 3 were the cleaved C-terminal and N-terminal fragments, respectively. Peak 4 was an impurity in the original substrate solution. Panel B shows the original fluorescence traces of different concentrations WT protease. The enzyme amounts were as follows: (a) 8.5; (b) 6.8; (c) 5.1; (d) 3.4; (e) 1.7 μg. The substrate (20 μM) itself was stable under the same conditions during the experimental period as shown in the baseline trace (f). Panel C show the initial rate of the change of fluorescence versus enzyme concentration. Panel D shows progress curves for the various mutant SARS proteases: (a) WT, 0.19 nmol; (b) R4A/E290A, 4.75 nmol (0.34 mg); (c) R4A, 0.19 nmol; (d) E290A, 4.75 nmol; (e) E290A, 0.19 nmol (yellow); (f) R4A/E290A, 0.19 nmol (green).

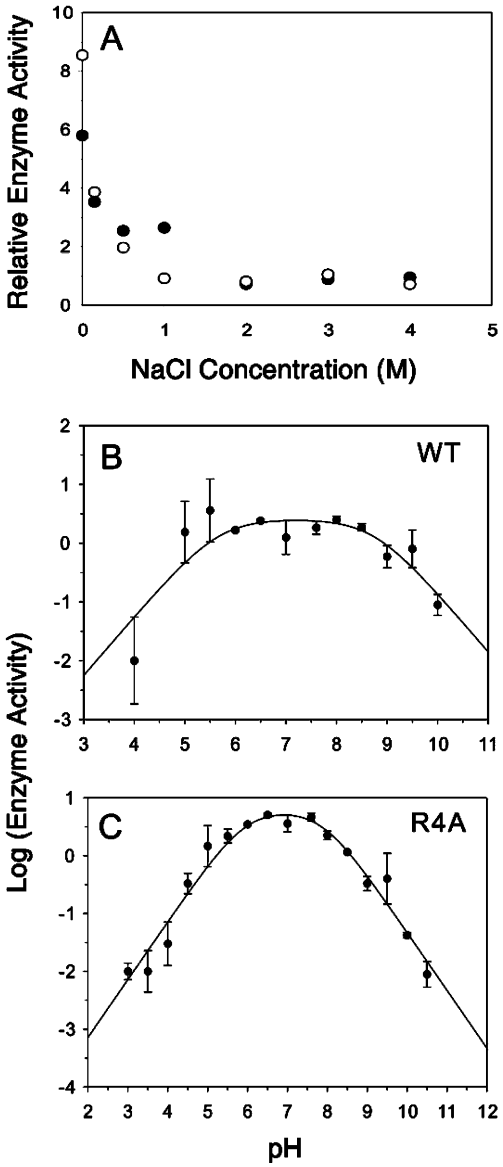

FIGURE 10: Effect of ionic strength and pH on the enzymatic activity of SARS-CoV main protease. Panel A shows relative enzyme activity versus NaCl concentration: (●) WT; (○) R4A mutant. Panels B and C show logarithm of the enzyme activity versus pH plots. The symbols are experimental data, and the curves are computer-generated results of fitting of the V_{max} values to pH according to an equation similar to eq 1 with the fitting residuals shown.

conventional HPLC method (*22*, *23*) and should be also more sensitive than the colorimetric method (*39*) for the SARS-CoV main protease. Some of the reliable kinetic parameters using the present method are summarized in Table 1.

The effect of mutation on enzymatic activity is obvious, especially at Glu-290. Both E290A and R4A/E290A mutants had negligible enzymatic activity (Figure 9C). The specific activities for WT, R4A, E290A, and R4A/E290A were 1930, 560, 0.26, and 0.42 U/mg, respectively. Among them, only WT and R4A mutant possessed high enough enzymatic activity for detailed kinetic analysis (Table 1 and Figure 10). Another domain III-deleted mutant (3CLc) was enzymatically inactive (Table 2).

Dependence of Enzymatic Activity of SARS-CoV Main Protease on Ionic Strength and pH. Both WT and R4A mutant were strongly inhibited by NaCl (Figure 10A). These

Table 2: Dimer−Monomer Association of the SARS-CoV Main Protease[a]

characteristics of the interfacial region	pH 6.0	pH 7.6	pH 8.0
protein data bank accession code	1UJ1	1UK3	1UK2
buried surface area (Å^2)	1114	1053	1121
energy gained upon association (kcal/mol)	−7.0	−10.3	−7.9
Salt Bridge Distance (Å) and Angle[b] (deg)			
Arg-4A NH2···Glu-290B OE1	2.84 (127)		
Arg-4A NH2···Glu-290B OE2			2.65 (107)
Glu-290A OE1···Arg-4B NH1			3.30 (132)
Glu-290A OE1···Arg-4B NH2	2.43 (173)	2.45 (159)	2.80 (156)
Dissociation Constant (nM)[c]			
WT (full length)	68 ± 10	89 ± 14	190 ± 14
3CLc (domain III-deleted mutant)	1778 ± 8	973 ± 197	991 ± 681

[a] Analyzed by the Protein Quaternary Structure File Server (*52*). [b] Numbers in parentheses are the salt bridge angle of N···O−C. [c] Obtained from sedimentation experiments, calculated and corrected to the standard conditions of pure water at 20 °C by the SEDPHAT program (*31*). The results are presented as mean ± standard errors.

results were consistent with the effect of NaCl on the quaternary structure and shape of the enzyme (Figure 5).

Figure 10B,C shows the effect of pH on the enzyme activity of WT and R4A mutant. Both WT and R4A showed bell-shaped activity−pH dependence. Fitting the experimental data to an equation similar to eq 1 obtained two apparent pK_a values the protonation of which affects the enzymatic activity. For WT, the apparent pK_{a_1} value of 5.7 ± 0.4 and pK_{a_2} value of 8.7 ± 0.4 were obtained. The former must be deprotonated and the latter must be protonated to obtain maximum enzyme activity. For the R4A mutant, these two apparent pK_a values were 5.9 ± 0.2 and 7.9 ± 0.2, respectively. In both WT and R4A mutant, the fitted lines in both acidic and basic sides had slopes approaching one indicating that only one protonation site was detectable in these cases.

DISCUSSION

Analytical ultracentrifugation (AUC) is a very powerful and reliable tool for characterizing the hydrodynamic and thermodynamic properties of macromolecules in solution (*28*, *40*). We have demonstrated that, among the biophysical probes, AUC plays a crucial role in differentiating polymerization versus the true unfolding intermediate (*41*, *42*). In the present report, again, we demonstrated that AUC is an essential tool in characterizing the quaternary structure of SARS-CoV main protease. This is extremely important for the SARS-CoV main protease since the monomer may be enzymatically inactive and substances that can intervene at the dimer interface may be used as potential anti-SARS-CoV drugs (*22*, *23*).

The crystal structure of the transmissible gastroenteritis (corona) virus (TGEV) main protease, which has been used as the template for modeling the theoretical three-dimensional structure of SARS-CoV main protease (*12*), revealed the same type of dimer. However, dynamic light scattering results indicated that both human coronavirus (HCoV) 299E and TGEV main protease exist as a mixture of monomer (65%) and dimer (35%) (*20*). The dimeric structure of SARS-

CoV main protease has been established by X-ray crystallographic studies (*18*). The difference per chain from the isolated subunit to dimer formation decreases a total sum of solvent accessible surface by approximately 1100 Å^2 in all pH values studied (Table 2), which is relatively small due to its steric arrangement (Figure 1A,B), but this solvent-accessible surface value is well above the cutoff value of 400 Å^2 used in differentiating crystal packing and subunit−subunit association. In this article, we provide conclusive evidence from sedimentation velocity experiments demonstrating that most of the protease molecules exist as a dimer in solution. The SARS-CoV main protease thus was established as a homodimer both in solid and in solution.

It should be noted that our protease preparation has a His_6-tag at the C-terminus. The recombinant SARS-CoV main protease prepared by Kuo et al. (*38*) does not have this His_6-tag, and they obtained a similar K_d value range for the dimer−monomer equilibrium to that reported in this paper. Furthermore, the 3CLc prepared by Shi et al. (*22*) does not have the His_6-tag, and our 3CLc has this tag, but both deletion mutants reach the same conclusion, the His_6-tag at the C-terminus does not seem to disturb the dimeric structure of the enzyme. Huang et al. (*39*) had demonstrated that the His_6-tag does not have any effect on the enzyme activity either.

We have also examined the behavior of the SARS-CoV main protease in solution by analytical size-exclusive chromatography. An unresolved monomer−dimer mixture was detected (Figure 8). The reason that monomeric SARS-CoV main protease was observed at 0.2 mg/mL at pH 7.6 by analytical size-exclusive chromatography in previous report could be due to dilution of the enzyme solution during elution from the column (*23*). A 10-fold dilution of the sample is quite possible in gel filtration chromatography, and the actual protein concentration is unpredictable. On the other hand, in AUC experiments, the protein concentration is under full control. In our case, the protein concentration determined externally is identical with those estimated from the UV absorbance of the AUC signals, which were used to double check the protein concentration according to the extinction coefficient of the enzyme calculated from its amino acid composition.

In their recent article, Shi et al. (*22*) provide experimental data showing the involvement of domain III in the dimerization of the SARS-CoV main protease. Independently, we reach a similar conclusion, and we provide the quantitative dissociation constants for the mutant with domain III deleted (3CLc) (Table 2). The 3CLc mutant that we produced possesses negligible enzyme activity.

We have further characterized the specific role of the ionic interaction in the interfacial region. The dissociation of the dimer in both acidic and basic pH environments suggests the involvement of two dissociable amino acid residues in the subunit interaction. There is an ionic pair, Arg-4···Glu-290, detected in all crystal forms of the SARS-CoV main protease (Table 2). Although the situation may be complex, the apparent pK_a values determined from these residues are reminiscent the Arg-4···Glu-290 ion pair (Figure 7). The apparent pK_a value of 5.0 is compatible with a glutamate carboxyl side chain, while an apparent pK_a value of 8.0 is smaller than that expected for an arginine guanidino side chain. This salt bridge is formed by protrusion of the N-terminus from subunit A to domain III of subunit B. Since Arg-4 is retained in 3CLc, it is more appropriate to compare the binding energy of 3CLc to E290A (Table 2). In that case, almost all of the binding energy of domain III is contributed by the Arg-4···Glu-290 ion pair. The dissociation constants of 3CLc (991 ± 681 nM) and E290A (970 ± 437 nM) are in the same range but with large standard errors even though thousands of data points were collected.

The conservation in sequence of the protein−protein interface region has been studied (see ref *43* and references therein). While Glu-290 is completely conserved among all coronavirus main proteases with known amino acid sequences, conservation of Arg-4 is less than 50%. Residue variety at Arg-4 includes lysine and valine. The lysine residue at position 5, on the other hand, is completely conserved. Mutation at either residue of the Arg-4···Glu-290 ion pair with the other charged residue remained (the single mutants) put a charged side chain in a hydrophobic environment and resulted in unstable dimers with large dissociation constants (Table 1). In the R4A/E290A double mutant, the smaller dissociation constant than any other single mutant may not be significant because of their large standard errors (Table 1). Since the R4A mutant has comparable enzymatic activity with WT and R4A has a large dissociation constant, dimer formation seems to not be the only factor that determines the enzyme activity.

The detailed kinetic enzymatic assay does not provide a conclusive result on the correlation between dissociation and enzyme activity. The R4A mutant is enzymatically as active as WT. The pH−activity profiles for both WT and R4A (Figure 10B,C) are similar. Interpretation of the kinetically determined apparent pK_a values is not straightforward. Because ionization of a basic residue is still observed in R4A, those apparent pK_a values determined by kinetics most likely reflect the catalytic dyad residues, His-41 and Cys-145 (see Figure 1A), and not the Arg-4···Glu-290 ion pair.

The 3D contours of the enzyme at three different pH values are shown in Figure 11. The whole molecule is negatively charged. Bioinformatics calculation indicates that the enzyme has a p*I* value of 6.2. However, under a physiological environment, the screen effect of salt will compensate a large fraction of the external negative potential. At pH 6.0, subunit B is in a conformation not suitable for catalysis and thus is inactive (*18*). The 3D contour of the protease at pH 6.0 is slightly different from those at pH 7.6 or 8.0 (Figure 11D).

The structural complementarity and electrostatic interactions between protein−protein interfaces have been extensively explored (*44*−*48*). The different interfaces can be designed to exploit electrostatic and hydrophobic forces in very different ways (*48*). Our experimental results indicate that ionic strength has a profound influence on the subunit interactions (Figure 5) and enzymatic activity (Figure 10A). These results suggest that the favorable electrostatic salt-bridge-like interactions are the major factor involved in the subunit association process (*49*) and the subunit interface is stabilized by an ionic interaction of the Arg-4···Glu-290 pair. It is conceivable that the enzyme is prone to dissociate at both acidic and alkali pH values. However, this is not reflected in the number of salt bridges in the interface. There are three ionic interactions between Arg-4 and Glu-290 at pH 8.0. These interactions are reduced to two at pH 6.0 and reduced further to one at pH 7.6 (Table 2). It is possible

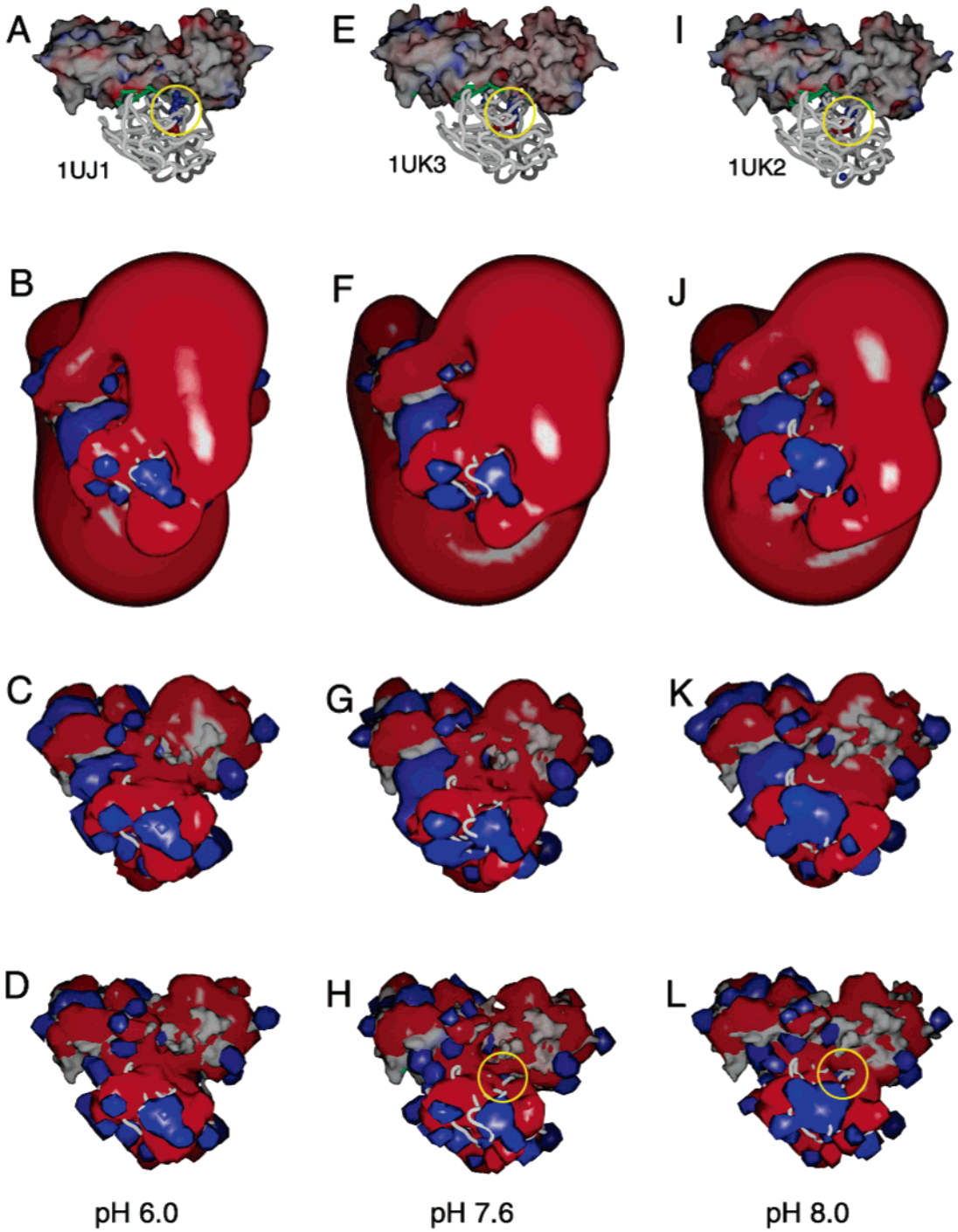

FIGURE 11: 3D-isopotential surface of the SARS-CoV main protease at different pH values: (A−D) pH 6.0 (pdb code 1UJ1); (E−H) pH 7.6 (pdb code 1UK3); (I−L) pH 8.0 (pdb code 1UK2). The surface model and 3D contours of the SARS-CoV main protease are displayed in the same scale and had equivalent orientation. In panels A, E, and I, one of the subunits is displayed in the surface model colored by the potential. The positive and negative areas are shown in blue and red, respectively. The Arg-4···Glu-290 ion pair is highlighted with a space filling model and circled in yellow. The 3D contours in panels B, F, and J are without salt. The univalent salt concentrations of 0.15 and 4 M are taken for 3D contours in panels C, G and K and panels D, H and L, respectively. The Arg-4 is visible in panels H and L (yellow circles).

that electrostatic complementarity rather than charge complementarity is a more appropriate parameter to describe the subunit−subunit interface of the SARS main protease (*45*). The more negative value of the difference in solvation energy of folding of the SARS-CoV main protease at pH 7.6 (Table 2) indicates a more hydrophobic character of the subunit−subunit interface upon assembly (*50*, *51*). Some of the hydrophobic interactions highlighted in Figure 1C are not observed at pH 6.0 or 8.0.

In summary, the Arg-4···Glu-290 ion pair has been demonstrated to play an important role in the subunit association. Dimerization of the subunits, however, may not be the only factor that determines the enzymatic activity of the SARS main protease.

ACKNOWLEDGMENT

We thank Dr. Shao-Hung Wang, Genome Research Center, National Yang-Ming University, Taipei, Taiwan,

Republic of China, for preparing the plasmid of SARS-CoV main protease. The authors also wish to express thanks to Dr. Lih-Hua Huang, Hepatitis Research Center, National Taiwan University Hospital, for providing information on the fluorogenic substrate.

REFERENCES

1. Chan, H. L., Tsui, S. K., and Sung, J. J. (2003) Coronavirus in severe acute respiratory syndrome (SARS), *Trends Mol. Med. 9*, 323−325.
2. Leng, Q., and Bentwich, Z. (2003) A novel coronavirus and SARS, *N. Engl. J. Med. 349*, 709.
3. Kuiken, T., Fouchier, R. A., Schutten, M., Rimmelzwaan, G. F., van Amerongen, G., van Riel, D., Laman, J. D., de Jong, T., van Doornum, G., Lim, W., Ling, A. E., Chan, P. K., Tam, J. S., Zambon, M. C., Gopal, R., Drosten, C., van der Werf, S., Escriou, N., Manuguerra, J. C., Stohr, K., Peiris, J. S., and Osterhaus, A. D. (2003) Newly discovered coronavirus as the primary cause of severe acute respiratory syndrome, *Lancet 362*, 263−270.
4. Rota, P. A., Oberste, M. S., Monroe, S. S., Nix, W. A., Campagnoli, R., Icenogle, J. P., Penaranda, S., Bankamp, B., Maher, K., Chen, M. H., Tong, S., Tamin, A., Lowe, L., Frace, M., DeRisi, J. L., Chen, Q., Wang, D., Erdman, D. D., Peret, T. C., Burns, C., Ksiazek, T. G., Rollin, P. E., Sanchez, A., Liffick, S., Holloway, B., Limor, J., McCaustland, K., Olsen-Rasmussen, M., Fouchier, R., Gunther, S., Osterhaus, A. D., Drosten, C., Pallansch, M. A., Anderson, L. J., and Bellini, W. J. (2003) Characterization of a novel coronavirus associated with severe acute respiratory syndrome, *Science 300*, 1394−1399.
5. Marra, M. A., Jones, S. J. M., Astell, C. R., Holt, R. A., Brooks-Wilson, A., Butterfield, Y. S. N., Khattra, J., Asano, J. K., Barber, S. A., Chan, S. Y., Cloutier, A., Coughlin, S. M., Freeman, D., Girn, N., Griffith, O. L., Leach, S. R., Mayo, M., McDonald, H., Montgomery, S. B., Pandoh, P. K., Petrescu, A. S., Robertson, A. G., Schein, J. E., Siddiqui, A., Smailus, D. E., Stott, J. M., Yang, G. S., Plummer, F., Andonov, A., Artsob, H., Bastien, N., Bernard, K., Booth, T. F., Bowness, D., Czub, M., Drebot, M., Fernando, L., Flick, R., Garbutt, M., Gray, M., Grolla, A., Jones, S., Feldmann, H., Meyers, A., Kabani, A., Li, Y., Normand, S., Stroher, U., Tipples, G. A., Tyler, S., Vogrig, R., Ward, D., Watson, B., Brunham, R. C., Krajden, M., Petric, M., Skowronski, D. M., Upton, C., and Roper, R. L. (2003) The Genome sequence of the SARS-associated coronavirus, *Science 300*, 1399−1404.
6. Tanner, J. A., Watt, R. M., Chai, Y. B., Lu, L. Y., Lin, M. C., Peiris, J. S., Poon, L. L., Kung, H. F., and Huang, J. D. (2003) The severe acute respiratory syndrome (SARS) coronavirus NTPase/helicase belongs to a distinct class of 5′ to 3′ viral helicases, *J. Biol. Chem. 278*, 39578−39582.
7. Stavrinides, J., and Guttman, D. S. (2004) Mosaic evolution of the severe acute respiratory syndrome coronavirus, *J. Virol. 78*, 76−82.
8. Eickmann, M., Becker, S., Klenk, H. D., Doerr, H. W., Stadler, K., Censini, S., Guidotti, S., Masignani, V., Scarselli, M., Mora, M., Donati, C., Han, J. H., Song, H. C., Abrignani, S., Covacci, A., and Rappuoli, R. (2003) Phylogeny of the SARS coronavirus, *Science 302*, 1504−1505.
9. Holmes, K. V. (2003) SARS coronavirus: a new challenge for prevention and therapy, *J. Clin. Invest. 111*, 1605−1609.
10. Kesel, A. J. (2003) A system of protein target sequences for anti-RNA-viral chemotherapy by a vitamin B6-derived zinc-chelating trioxa-adamantane-triol, *Bioorg. Med. Chem. 11*, 4599−4613.
11. Thiel, V., Ivanov, K. A., Putics, A., Hertzig, T., Schelle, B., Bayer, S., Weissbrich, B., Snijder, E. J., Rabenau, H., Doerr, H. W., Gorbalenya, A. E., and Ziebuhr, J. (2003) Mechanisms and enzymes involved in SARS coronavirus genome expression, *J. Gen. Virol. 84*, 2305−2315.
12. Anand, K., Ziebuhr, J., Wadhwani, P., Mesters, J. R., and Hilgenfeld, R. (2003) Coronavirus main proteinase (3CLpro) structure: basis for design of anti-SARS drugs, *Science 300*, 1763−1767.
13. Chou, K. C., Wei, D. Q., and Zhong, W. Z. (2003) Binding mechanism of coronavirus main proteinase with ligands and its implication to drug design against SARS, *Biochem. Biophys. Res. Commun. 308*, 148−151.
14. Pergament, I., Reich, R., and Srebnik, M. (2002) Novel matrix metallo-proteinase (MMP-2) phosphonoboronate inhibitors, *Bioorg. Med. Chem. Lett. 12*, 1215−1218.
15. Krausslich, H. G., and Wimmer, E. (1988) Viral proteinases, *Annu. Rev. Biochem. 57*, 701−754.
16. Bianchi, E., and Pessi, A. (2002) Inhibiting viral proteases: challenges and opportunities, *Biopolymers 66*, 101−114.
17. Tong, L. (2002) Viral proteases, *Chem. Rev. 102*, 4609−4626.
18. Yang, H., Yang, M., Ding, Y., Liu, Y., Lou, Z., Zhou, Z., Sun, L., Mo, L., Ye, S., Pang, H., Gao, G. F., Anand, K., Bartlam, M., Hilgenfeld, R., and Rao, Z. (2003) The crystal structures of severe acute respiratory syndrome virus main protease and its complex with an inhibitor, *Proc. Natl. Acad. Sci. U.S.A. 100*, 13190−13195.
19. Ziebuhr, J., Bayer, S., Cowley, J. A., and Gorbalenya, A. E. (2003) The 3C-like proteinase of an invertebrate nidovirus links coronavirus and potyvirus homologs, *J. Virol. 77*, 1415−1426.
20. Anand, K., Palm, G. J., Mesters, J. R., Siddell, S. G., Ziebuhr, J., and Hilgenfeld, R. (2002) Structure of coronavirus main proteinase reveals combination of a chymotrypsin fold with an extra alpha-helical domain, *EMBO J. 21*, 3213−3224.
21. Hegyi, A., Friebe, A., Gorbalenya, A. E., and Ziebuhr, J. (2002) Mutational analysis of the active centre of coronavirus 3C-like proteases, *J. Gen. Virol. 83*, 581−593.
22. Shi, J., Wei, Z., and Song, J. (2004) Dissection study on the SARS 3C-like protease reveals the critical role of the extra domain in dimerization of the enzyme: Defining the extra domain as a new target for design of highly specific protease inhibitors, *J. Biol. Chem. 279*, 24765−24773.
23. Fan, K., Wei, P., Feng, Q., Chen, S., Huang, C., Ma, L., Lai, B., Pei, J., Liu, Y., Chen, J., and Lai, L. (2004) Biosynthesis, purification, and substrate specificity of severe acute respiratory syndrome coronavirus 3C-like proteinase, *J. Biol. Chem. 279*, 1637−1642.
24. Braman, J., Papworth, C., and Greener, A. (1996) Site-directed mutagenesis using double-stranded plasmid DNA templates, *Methods Mol. Biol. 57*, 31−44.
25. Whitmore, L., and Wallace, B. A. (2004) DICHROWEB, an online server for protein secondary structure analyses from circular dichroism spectroscopic data, *Nucleic Acids Res. 32*, W668−W673.
26. Lobley, A., Whitmore, L., and Wallace, B. A. (2002) DICHROWEB: an interactive website for the analysis of protein secondary structure from circular dichroism spectra, *Bioinformatics 18*, 211−212.
27. Schuck, P. (2000) Size-distribution analysis of macromolecules by sedimentation velocity ultracentrifugation and Lamm equation modeling, *Biophys. J. 78*, 1606−1619.
28. Lebowitz, J., Lewis, M. S., and Schuck, P. (2002) Modern analytical ultracentrifugation in protein science: a tutorial review, *Protein Sci. 11*, 2067−2079.
29. Schuck, P., Perugini, M. A., Gonzalez, N. R., Howlett, G. J., and Schubert, D. (2002) Size-distribution analysis of proteins by analytical ultracentrifugation: strategies and application to model systems, *Biophys. J. 82*, 1096−1111.
30. Dam, J., and Schuck, P. (2004) Calculating sedimentation coefficient distributions by direct modeling of sedimentation velocity concentration profiles, *Methods Enzymol. 384*, 185−212.
31. Schuck, P. (2003) On the analysis of protein self-association by sedimentation velocity analytical ultracentrifugation, *Anal. Biochem. 320*, 104−124.
32. Holskin, B. P., Bukhtiyarova, M., Dunn, B. M., Baur, P., de Chastonay, J., and Pennington, M. W. (1995) A continuous fluorescence-based assay of human cytomegalovirus protease using a peptide substrate, *Anal. Biochem. 226*, 148−155.
33. Bonneau, P. R., Plouffe, C., Pelletier, A., Wernic, D., and Poupart, M. A. (1998) Design of fluorogenic peptide substrates for human cytomegalovirus protease based on structure−activity relationship studies, *Anal. Biochem. 255*, 59−65.
34. Sun, H., Luo, H., Yu, C., Sun, T., Chen, J., Peng, S., Qin, J., Shen, J., Yang, Y., Xie, Y., Chen, K., Wang, Y., Shen, X., and Jiang, H. (2003) Molecular cloning, expression, purification, and mass spectrometric characterization of 3C-like protease of SARS coronavirus, *Protein Expression Purif. 32*, 302−308.
35. Mao, D., Wachter, E., and Wallace, B. A. (1982) Folding of the H^+-ATPase proteolipid in phospholipid vesicles, *Biochemistry 21*, 4960−4968.
36. Sanchez del Pino, M. M., and Fersht, A. R. (1997) Nonsequential unfolding of the α/β barrel protein indole-3-glycerol-phosphate synthase, *Biochemistry 36*, 5560−5565.

37. Bacha, U., Barrila, J., Velazquez-Campoy, A., Leavitt, S. A., and Freire, E. (2004) Identification of novel inhibitors of the SARS coronavirus main protease 3CL(pro), *Biochemistry 43*, 4906−4912.
38. Kuo, C. J., Chi, Y. H., Hsu, J. T. A., and Liang, P. H. (2004) Characterization of SARS main protease and inhibitor assay using a fluorogenic substrate, *Biochem. Biophys. Res. Commun. 318*, 862−867.
39. Huang, C., Wei, P., Fan, K., Liu, Y., and Lai, L. (2004) 3C-like Proteinase from SARS coronavirus catalyzes substrate hydrolysis by a general base mechanism, *Biochemistry 43*, 4568−4574.
40. Laue, T. M., and Stafford, W. F., 3rd. (1999) Modern applications of analytical ultracentrifugation, *Annu. Rev. Biophys. Biomol. Struct. 28*, 75−100.
41. Chang, H. C., Chou, W. Y., and Chang, G. G. (2002) Effect of metal binding on the structural stability of pigeon liver malic enzyme, *J. Biol. Chem. 277*, 4663−4671.
42. Chang, H. C., and Chang, G. G. (2003) Involvement of single residue tryptophan 548 in the quaternary structural stability of pigeon cytosolic malic enzyme, *J. Biol. Chem. 278*, 23996−24002.
43. Caffrey, D. R., Somaroo, S., Hughes, J. D., Mintseris, J., and Huang, E. S. (2004) Are protein−protein interfaces more conserved in sequence than the rest of the protein surface? *Protein Sci. 13*, 190−202.
44. Lawrence, M. C., and Colman, P. M. (1993) Shape complementarity at protein/protein interfaces, *J. Mol. Biol. 234*, 946−950.
45. McCoy, A. J., Chandana Epa, V., and Colman, P. M. (1997) Electrostatic complementarity at protein/protein interfaces, *J. Mol. Biol. 268*, 570−584.
46. Xu, D., Tsai, C. J., and Nussinov, R. (1997) Hydrogen bonds and salt bridges across protein−protein interfaces, *Protein Eng. 10*, 999−1012.
47. Lo Conte, L., Chothia, C., and Janin, J. (1999) The atomic structure of protein−protein recognition sites, *J. Mol. Biol. 285*, 2177−2198.
48. Sheinerman, F. B., and Honig, B. (2002) On the role of electrostatic interactions in the design of protein−protein interfaces, *J. Mol. Biol. 318*, 161−177.
49. Mayo, K. H., and Chen, M. J. (1989) Human platelet factor 4 monomer−dimer−tetramer equilibria investigated by ^{1}H NMR spectroscopy, *Biochemistry 28*, 9469−9478.
50. Eisenberg, D., and McLachlan, A. D. (1986) Solvation energy in protein folding and binding, *Nature 319*, 199−203.
51. Chiche, L., Gregoret, L. M., Cohen, F. E., and Kollman, P. A. (1990) Protein model structure evaluation using the solvation free energy of folding, *Proc. Natl. Acad. Sci. U.S.A. 87*, 3240−3243.
52. Henrick, K., and Thornton, J. M. (1998) PQS: a protein quaternary structure file server, *Trends Biochem. Sci. 23*, 358−361.
53. Kraulis, P. J. (1991) MOLSCRIPT: a program to produce both detailed and schematic plots of protein structures, *J. Appl. Crystallogr. 24*, 946−950.
54. Merritt, E. A., and Bacon, D. J. (1997) Raster3D: photorealistic molecular graphics, *Methods Enzymol. 277*, 505−524.
55. Wallace, A. C., Laskowski, R. A., and Thornton, J. M. (1995) LIGPLOT: a program to generate schematic diagrams of protein−ligand interactions, *Protein Eng. 8*, 127−134.

BI0490237